

Beric Skews

Shock wave interaction with porous plates

Received: 6 December 2004 / Revised: 25 May 2005 / Accepted: 30 June 2005 / Published online: 9 August 2005
© Springer-Verlag 2005

Abstract Previous detailed studies of the interaction of a shock wave with a perforated sheet considered the impact of a shock wave on a plate with regularly spaced slits giving area blockages of 60 and 67%, at various angles of incidence, and resulting in both regular and Mach reflection. The current work extends this study to a much wider variety of plate geometries. Blockage ratios of 20, 25, 33, 50, and 67 and inclinations of 45, 60, 75, and 90° to the shock wave were tested. Four different thicknesses of plate were tested at the same frontal blockage in order to assess the effects of gap guidance. Tests were conducted at two shock Mach numbers of 1.36 and 1.51 (inverse pressure ratios of 0.4 and 0.5). It is found that secondary reflected and transmitted waves appear due to the complex interactions within the grid gaps, and that the vortex pattern which is generated under the plate is also complex due to these interactions. The angle of the reflected shock, measured relative to the plate, decreases with plate blockage and the angle of inflow to the plate reduces with increasing blockage. By analysing the flow on the underside of the plate the pseudo-steady flow assumption is found to be a reasonable approximation. Both the pressure difference and the stagnation pressure loss across the plate are evaluated. It is found that over the range tested the plate thickness has a minimal effect.

Keywords Shock wave reflection · Refraction · Porous material · Perforated plates · Vortex sheets

1 Introduction

The earliest quantitative study of the interaction of a shock wave with a perforated plate is that of Friend

(1958). In his tests, plates were drilled with holes uniformly distributed over the surface to give a blockage ratio of 50%. The plate was 3 mm thick and the holes 6 mm in diameter. Sufficiently strong shock waves were used in most tests so that the flow choked as it passed through, thereby giving a useful boundary condition for a theoretical treatment. It was also assumed that tangential momentum was conserved across the plate. Studies on a plate with slits by Onodera and Takayama (1990) have been conducted to establish the conditions for transition from Mach to regular reflection of the shock wave. They started with conditions of glancing incidence until regular reflection was established. The main assumption in the accompanying theoretical treatment was that the flow into the plate was normal to its surface.

These latter studies were extended to regular reflection with incidence angles up to head-on reflection (Skews and Takayama 1996). Associated studies are reviewed in this latter work. This study demonstrated that a number of assumptions made in earlier work are in error. The most marked of these is that the inflow through the plate is not normal to the surface, except for the special case of head-on impact (0° incidence angle). In fact, for shock incidence angles between 30 and 90°, the angle of inflow is shown to be strongly inclined to the surface, at an angle of about 17°, for the particular plate geometry tested. This inflow angle appeared to be independent of Mach number over an incident shock Mach number range from 1.18 to 1.54. A plane transmitted wave is generated on the underside of the plate due to the coalescence of wavelets coming through the slits. This is followed by a complex vortex pattern whose leading edge position is compatible with the strength of the transmitted wave using the assumption of pseudo-steady flow and uniform regions between the features.

Application of these findings range from flow through protective barriers, losses through porous screens, and devices such as wave rotors. The latter are being studied as a potential route to higher specific power and lower specific fuel consumption in gas turbines. One of the problems in predicting performance is

B. Skews
School of Mechanical, Industrial, and Aeronautical Engineering,
University of the Witwatersrand,
PO WITS, 2050 Johannesburg, South Africa
E-mail: bskews@mech.wits.ac.za

to evaluate the losses. Flow into these rotors is often at very large angles of attack impinging on what is essentially a grid of flat plates. The similarity with the flow induced behind an impinging oblique shock on a plate is obvious and attempts to use shock induced flow tests, such as the one above, to ascertain these losses have been made (Wilson et al. 1998).

The purpose of the current study is to add to the body of data in the field, and particularly to extend and more accurately evaluate the effect of blockage on the flow. Due to different measurement techniques employed in the current study features not previously noted have also been identified. In the case of regular reflection where the reflection point is not influenced by a corner signal the flow can be treated as being pseudo-steady, and the results from transient reflection tests may be applied to the equivalent steady flow situation, in this case a steady flow approaching a grid at an angle.

2 Experimental procedure

The plate geometry used is shown in Fig. 1. It consists of a series of bars each of width t , and depth l , positioned at a pitch b . For general applications the important flow parameters are the inflow velocity, V_2^* , and inflow angle, ϵ , which for shock interaction applications are a result of the incident shock Mach number and angle of incidence.

Table 1 identifies the geometry of the grid assemblies that were tested. It should be noted that these are split into two groups. In the first five the plate thickness and the bar width are kept constant whilst the pitch is changed, giving variations in the blockage ratio from 20 to 67%. The last three entries plus the third entry give four test pieces with the same blockage ratio of 33%, but with varying plate thicknesses, in order to determine any effects of crossbar aspect ratio.

All grids were tested at incident shock Mach numbers of 1.36 and 1.51 (inverse pressure ratios of 0.5 and 0.4). Grid angles were set at 45, 60, 75, and 90°, because regular reflection tests were required, mainly to isolate the reflection point from the corner signal arising from

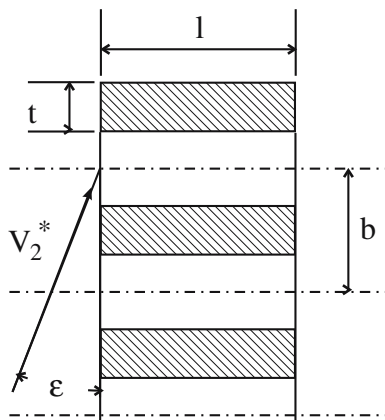


Fig. 1 Grid geometry

Table 1 Grid geometry

Width t mm	Pitch b mm	Blockage %	Thickness l mm
1.2	6.0	20	3.6
1.2	4.8	25	3.6
1.2	3.6	33	3.6
1.2	2.4	50	3.6
1.2	1.8	67	3.6
1.2	3.6	33	2.4
1.2	3.6	33	4.8
1.2	3.6	33	6.0

the front of the test section and therefore to represent the general case of uniform compressible flow through slits. Furthermore, the Mach reflection case, with its non-uniform flow regions, has received more study (Onodera and Takayama 1990). The grids were fabricated from thin rectangular bars cut from brass (1.2 mm thick and 70 mm long, and widths corresponding to the plate thicknesses given in Table 1). These were glued into edge bars 3 mm wide with machined slots at a pitch to give the correct blockage ratio. This meant that the edges of the grid had a solid strip 3 mm wide, which results in a small part of the incident wave reflecting off it which has to be accounted for when doing measurements, as well as some additional interactions which need to be understood when interpreting the shadowgraphs, as will be discussed later. The grid assemblies were attached to a circular arc supporting frame fitted in a mating frame so that the incidence angle of the plate could be varied. A schematic of the arrangement is shown in Fig. 2.

The tests were conducted in a standard shock tube. It consists of a 2 m long driver section, a 6 m driven section and a 300 mm long test section. The test section is rectangular in cross-section and has a height of 180 mm and a width of 76.2 mm. The shock wave which reaches the test section is free from irregularities, except some very weak transverse waves, and the testing time is completed before any contact surfaces or reflected waves reach the test section from the upstream end. Mach

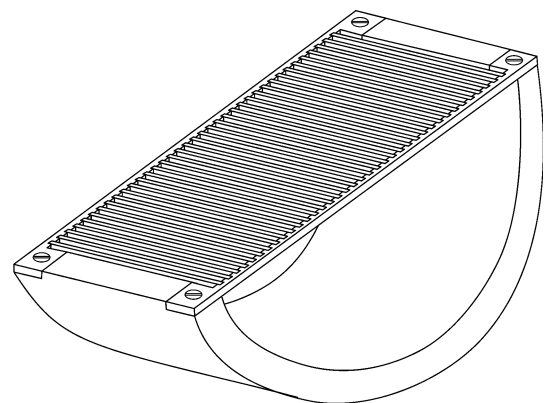


Fig. 2 Test piece arrangement

numbers are reproducible to within ± 0.02 . The ambient atmospheric pressure in the tube before firing, for all tests, was 0.83 bar.

Contact shadowgraph techniques were used to capture images of the wave pattern. This technique is half a standard shadowgraph setup with the film placed in contact with the test section window. A Xenon flash tube with a flash duration of $1 \mu\text{s}$ was used as the light source. The flash is positioned at the focal point of a parabolic mirror so that parallel light passes through the test section directly onto the film. The images were captured on quarter plate negative material and thus record an image at full size. Images were then scanned on a calibrated digital scanner at 1,200 dpi and imported into CAD (Computer Aided Design) software having facilities for zooming onto features of interest and enabling accurate scaling and measurement. Angular measurement resolution was set to 0.1° . This is suitable where distinct lines of shock waves (such as the incident wave) and the plate surface (at the two ends) are visible. For others, such as the transmitted and reflected waves, visual estimates were made of the best fit straight line in the central portion of the wave where the curved waves from the grids have merged and before the effects of the corner signal cause wave curvature, as will be discussed later. It is noted that the reflected and transmitted wave in the region near the reflection point can lie ahead of the straight section of the wave after the individual wavelets merge, presumably due to the effects of the gap restriction. Measurement of the line of vortices is the least accurate. However, whether the line is measured through the centre of the black features of the vortices on the image or tangent to them the angle will not be much affected because all the primary vortex images are much the same size.

3 Analysis

The flow properties were determined using two frames of reference, one fixed in the reflection point and one fixed

in the plate, as done in the earlier study (Skews and Takayama 1996), and as indicated in Fig. 3.

Velocities with asterisks are those relative to the plate, and those without are relative to the reflection point D. V_D is the velocity with which the reflection point moves up the plate. I, R, and T, represent the incident, reflected, and transmitted waves respectively. The arrowed lines represent the pseudo-steady streamlines for an observer stationary with respect to the reflection point D. C is the contact surface separating the gas, originally below the plate, and which has been engulfed by the transmitted shock (region 4), from that which has flowed through the plate (region 3). It is visible as a line of vortices. The gas velocities relative to the plate and behind the incident and transmitted waves, V_1^* and V_4^* , are normal to these waves. Parameters in region (1) are determined from the known incident shock Mach number and incidence angle using standard oblique shock relations. Conditions in region (2) can be similarly determined from the measured angle of reflection and the known conditions in state (1). The Mach number of the transmitted wave is determined from its angle to the plate and the velocity of point D, and conditions behind it can thus also be calculated. The direction of the absolute velocity relative to the reflection point, V_4 , (pseudo-steady frame) will be parallel to the contact surface if the flow in region (4) is uniform. This was found to be so in the earlier work (Skews and Takayama 1996). In addition it was found, from studying the vortex trajectories passing through the plate, that the flow emerging from the plate is perpendicular to it, relative to the plate. Furthermore the absolute velocity in region (3) should also be parallel to the contact surface. These factors enable the complete velocity triangle in region (3) to be determined, which then establishes the magnitude of V_3 . The same techniques are applied in this study.

For head-on impact different measurements are necessary, and a different set of equations used since there are no angle measurements. The main features are the distance from the front surface of the plate to each of the incident wave, the reflected wave, the transmitted wave, and the line of the vortices. Simple one-dimensional shock theory for impact on a permeable interface is then applied, again assuming uniform states between the features in order to calculate the pressures and velocities in the equivalent regions to those in Fig. 3. In the head-on case Region (1) is that behind the incident wave, region (2) that between the reflected wave and the face of the specimen, region (3) that between the line of vortices and the back of the plate, and region (4) that between the transmitted wave and the vortices. Since no information is available on the changes of velocity through the grid itself, these data are subject to larger errors since the wave and gas velocities are calculated as average values from the moment the incident shock strikes the front surface.

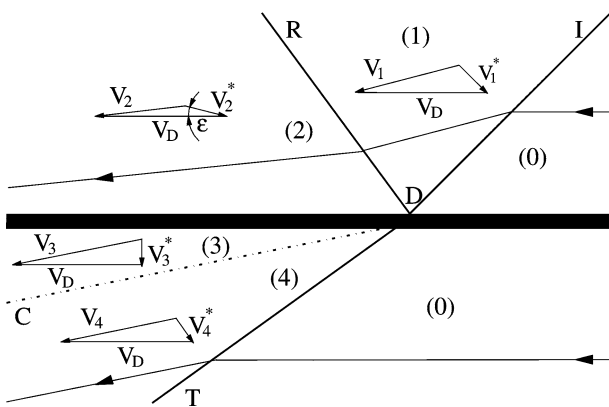


Fig. 3 Velocity triangles connecting frames of reference

4 Observations of flow phenomena

4.1 General flow features

A typical set of shadowgraphs is given in Fig. 4. The numbers in the caption refer to nominal wall angle, percentage blockage, and incident shock Mach number. Such images are analysed as indicated in Sect. 3.

Although flow features vary in detail depending on the initial conditions there are a number which may be readily identified. These are shown schematically in Fig. 5. In many cases the reflected wave appears as a double line. The outermost line is the weak shock that is reflected off the 3 mm wide rib mounting frames adjacent to the window and should be ignored in evaluating the flow field. This effect will not influence the central two-dimensional part of the flow. As in the case of regular reflection of a planar shock wave from a wedge, the reflected shock wave is curved over a segment which can receive signals from the corner. However, immediately behind the reflection point the flow is supersonic relative to it and the flow is unaware of the presence of the corner, and the reflected wave is planar. These two regions of flow are separated by a corner signal which is clearly visible in the images. For the grid flow under consideration this first corner signal is followed by similar corner signals arising from each of the grid bars, as shown in Fig. 5. The flow of interest is that between the first corner signal and the point of reflection. An interesting case is that of the first image in Fig. 4 since for the Mach number and wall angle shown regular reflection is not possible on an impermeable wall. This is indicated by the wave reflecting off the support bars being curved along its whole length. However, for the permeable wall the reflection is regular and the corner signal is evident. In some of the images, a similar corner signal is evident on the downstream side due to the interaction of the transmitted shock wave with the grid holder.

It is clear from the photographs that both the reflected shock and the transmitted shock result from the merging of waves reflected and transmitted from the individual grid elements. These waves are roughly semi-circular in shape as they propagate outwards into the surrounding flow. Measurements of the wave angles for these waves are taken where these wavelets have merged into a planar wave. In Skews and Takayama (1996) the waves on the upper surface were used as an independent means of estimating the inflow into the plate, assuming that they were sonic and circular and graphically locating the center of the circle, which convects at the flow velocity.

A second (and in some cases a third and fourth) reflection is noted in some of the images. These secondary waves result from complex interactions within the grid and can thus vary depending on the Mach number, blockage, grid length, and inclination. Similar secondary waves are also sometimes noted on the underside of the plate and can be discerned in the first

image of Fig. 4. These additional waves were not identified at all in the earlier interferometric study (Skews and Takayama 1996), this indicating a significant benefit in the use of contact shadowgraphy for the identification of weak waves. A complex array of vortices are also shed during the interaction. The first row were surmised in the earlier work to be due to shock diffraction at the entry to the slits arising from the inclined flow entry. This is incorrect, as will be shown later, and the vortex development is significantly more complex.

Some of the effects of Mach number can be inferred directly from comparison of images. Figure 6 compares the images on the 50% blockage grid, with the upper half the result for a Mach number of 1.36 and the lower half at 1.51. Both pictures were taken 40 μ s after shock impact. Interestingly, the reflected waves have moved the same distance back upstream but that for the Mach 1.51 case is stronger because it is moving into the gas flow induced behind the incident wave, which has a higher velocity. On the downstream side both the transmitted wave and the flow through the grid, as identified from the contact surface, have higher velocities for the stronger shock.

4.2 Flow in the gaps

In order to help to clarify more of the detail of the flow through the grid so as to understand better the development of the additional waves, as well as the vortex formation, a number of tests were conducted with 6 mm deep crossbars. Since the support plate is only 3 mm deep this enables part of the flow between the bars to be visualised. Figure 7 shows sections of these flows, the first with the visible part of the gaps above the support bars and the other two with the plate inverted.

The separation of the flow at the top of the front face of each crossbar is clearly visible in the first image and clearly shows the development of a vortex in each gap resulting from the shock diffraction. This vortex then migrates down into the gap although a separation bubble remains attached at the inlet, very soon becoming fixed in profile as the flow tends to become pseudo-steady. It is noted that when the crossbars extend above the support bar, the reflection from the support is lower than the main reflection, as is to be expected. It is also clear from the first image that the first row of vortices does not originate at the upper face: extrapolating the line of vortices back to the under-surface of the plate indicates that it is generated there. The supposition that these vortices were the result of the entering flow, made in the earlier work (Skews and Takayama 1996), is thus incorrect. This is confirmed in the latter two images, where it is clear that these vortices arise as the shock passing through the gap diffracts at the rear corner of the exit between crossbars. This also means that this vortex rotation is counter-clockwise. Some appreciation of the complex flow within the gap showing a series of transverse waves and Mach reflections as well as this

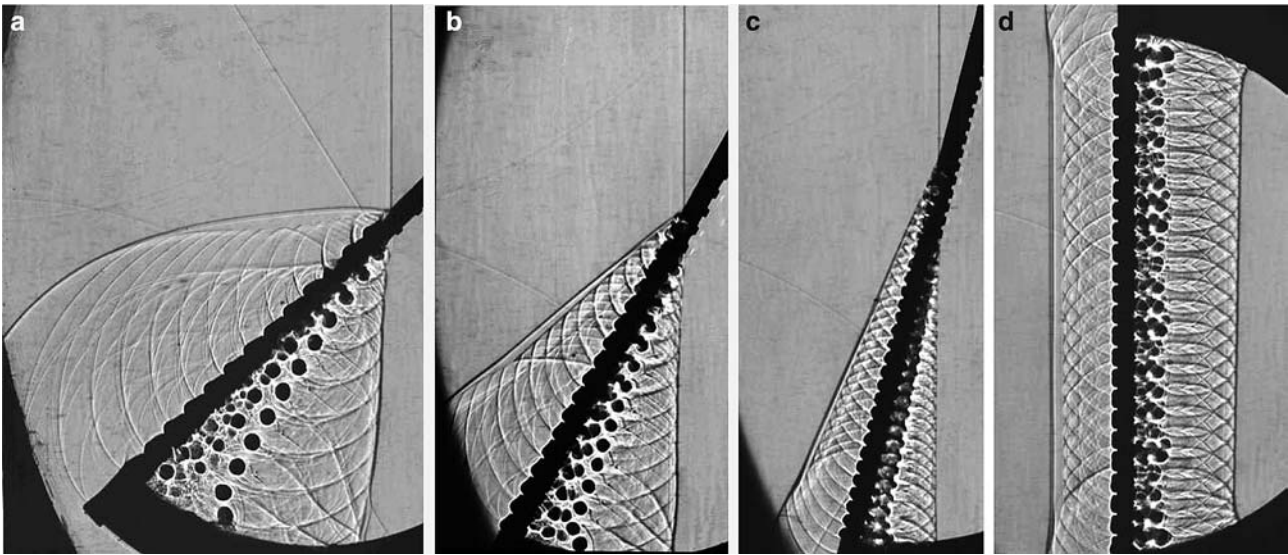


Fig. 4 Typical shadow images for various wall angles, percentage blockage, and Mach number. **a** 45°, 25%, $M = 1.367$, **b** 60°, 33%, $M = 1.352$, **c** 75°, 50%, $M = 1.359$, **d** 90°, 33%, $M = 1.508$

vortex formation is clear in the last image. Furthermore, it is evident that further vortices are shed at the gap exit before the arrival of the entry starting vortex at the plate exit. The detailed nature of these flows and the vortex streets generated will depend on the grid geometry, plate angle, and Mach number. A more detailed examination would probably best be done using CFD.

A revised suggestion of the interaction is given in Fig. 8 including both the vortex sets described above as well as the semi-circular waves evident above and below the plate. A simple evaluation of how these waves behave within the gap helps to identify the cause of the secondary waves noted in many of the photographs and sketched in Fig. 5. These arise due to the reflection of the initial approximately semi-circular reflected shock from a crossbar re-reflecting from a preceding bar. It is evident that these reflections within the gaps will result in complex flows.

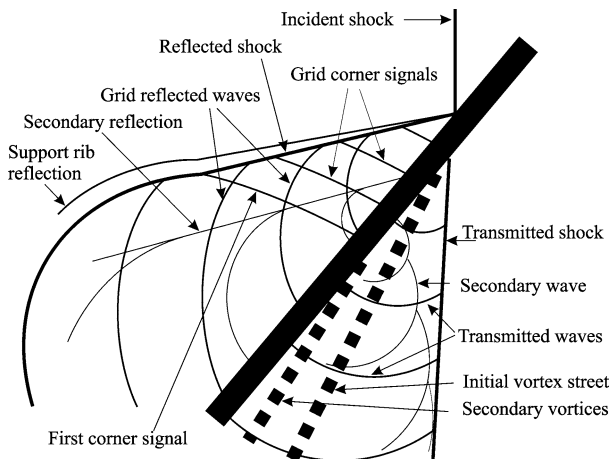


Fig. 5 The main features of the flow

5 Results and discussion

5.1 Flow above the plate

For tests to determine the effects of blockage the crossbars were kept at a depth of 3.6 mm and the spacing changed to give blockages as specified in Table 1. The first important parameter to consider is the effect of blockage on the angle of reflection. It is known from earlier work [see the review and results in (Skews and Takayama 1996)] that wall roughness and permeability both reduce the angle of reflection; in one case because of the virtual inflow due to an effective negative displacement thickness of the boundary layer and in the

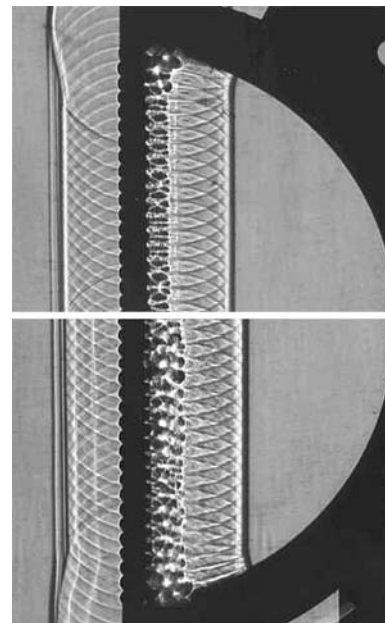


Fig. 6 Effects of Mach number on the propagation through a 90° grid. *Top* $M = 1.36$, *Bottom* $M = 1.51$

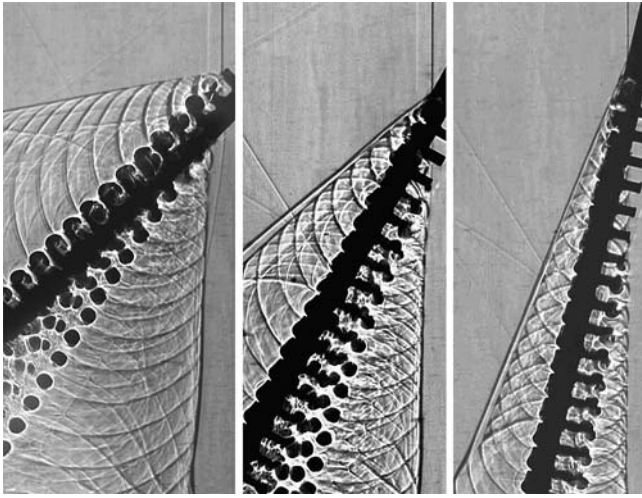


Fig. 7 Flow effects within the grid

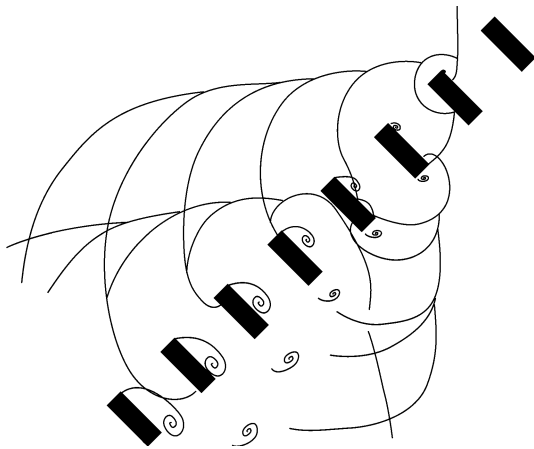


Fig. 8 Inferred development of secondary waves and vortices

other due to actual inflow. However, for porous walls the effect has previously been noted but has not been quantified. Figure 9 gives the results for the present tests and the two Mach numbers used.

As expected the experimental points lie between the limits of regular reflection off an impermeable wall, corresponding to 100% blockage and calculated using oblique shock relations, and that for 0% blockage calculated for the reflected wave being a sound wave. There is a clear and consistent correlation, with increasing blockage resulting in higher reflection angles. It is also interesting to note that regular reflection is obtained for all tests on the 45° wall where this is impossible for an impermeable wall, and Mach reflection occurs instead. Permeability thus clearly delays transition from regular to Mach reflection. From the current data set it is not possible to determine the detachment angle between the reflection types as a function of blockage. As the blockage decreases so the experimental points tend to

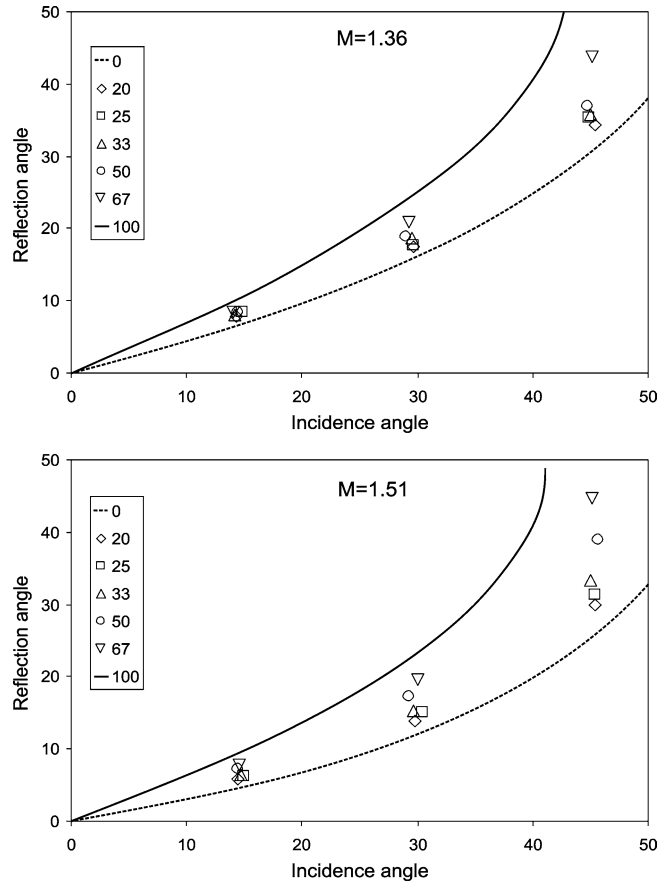


Fig. 9 Effect of percentage blockage on reflection angle

group so that going from 25 to 33% causes a much smaller change in reflection angle than going from 50 to 67%.

As identified in Sect. 1 a number of earlier studies had assumed that the inflow would be perpendicular to the front face of the grid; until it was shown in Skews and Takayama (1996) that it was significantly inclined to the surface. That work, however, could not ascertain the effects of plate blockage since the two grids tested had similar values (60 and 67%). This was an unexpected result and was part of the motivation for conducting the present study. The new results are given in Fig. 10.

In all cases except that of head-on impact these results show significant inclination of the flow at the inlet to the plate with respect to the plate surface. The inflow angle is always less than the wall angle (the dashed line shows this case). If they were equal this would mean that the inlet flow is in the same direction as the propagation direction of the incident shock (or V_1^* , Fig. 3) which could only happen if the reflected wave were a sound wave, i.e. no blockage.

The result of this angled inflow is the development of a separation bubble on the upstream corners of the gaps in the grid, as is evident in Figs. 7 and 8. The variation of angle with blockage is presented in Fig. 11. There is a decrease in inflow angle as blockage increases, as is to be

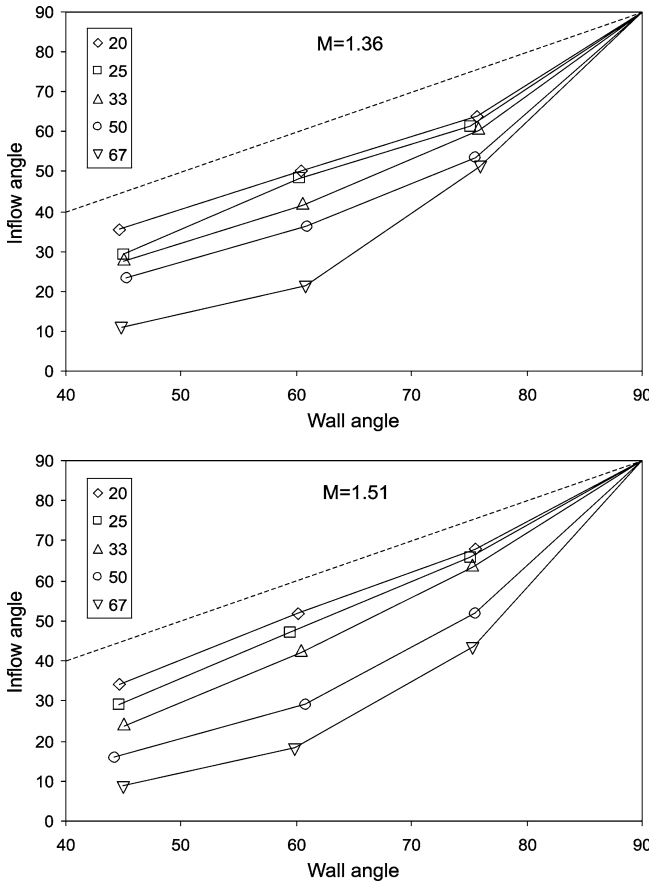


Fig. 10 Inflow angle, ϵ

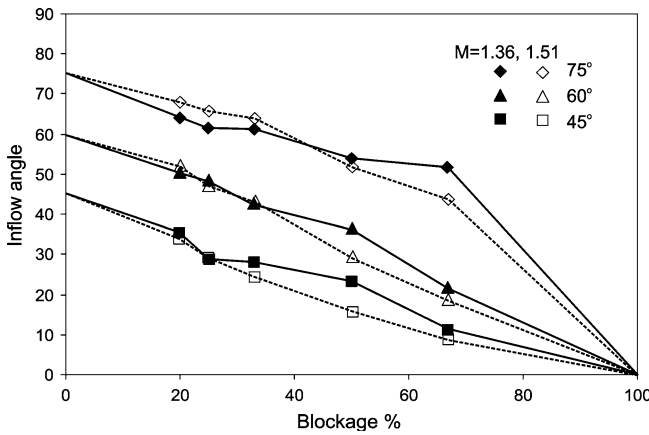


Fig. 11 The effect of blockage on inflow angle

expected due to greater resistance to flow through the grid, although there is some sign of flattening out of the curves for the weaker shock in the mid-range of blockages. In the case of zero blockage the inflow angle is simply the plate angle.

The non-dimensional inflow velocities are given in Fig. 12 for the $M = 1.51$ case. The $M = 1.36$ case shows identical trends. Both the absolute velocity, V_2^*/a_0 , and

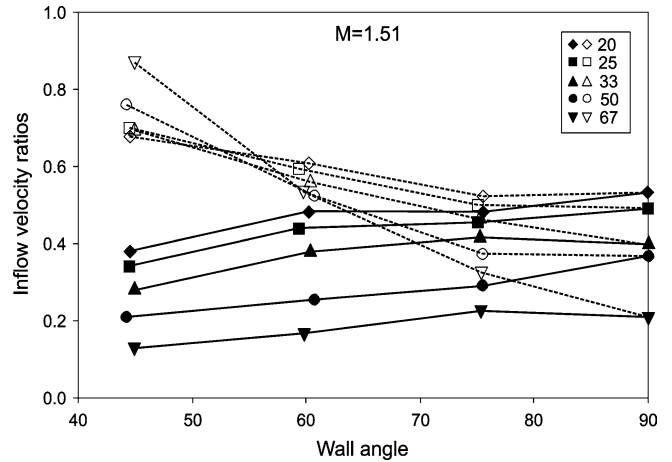


Fig. 12 Absolute velocity (*dotted lines*) and normal component (*solid lines*) of the inflow velocity

its component normal to the surface, v_2^*/a_0 , are shown. They are the same for the 90° wall. The normal component simply increases in magnitude as the surface becomes more permeable, and increases slightly with increase in wall angle. The behaviour of the absolute velocity is somewhat different, in that it increases with increased blockage at small wall angles (45°) but decreases with increased blockage at large angles (75 and 90°). It remains almost constant for the 60° wall. There is thus a complex interplay between reflected shock angle and the corresponding driving pressure in region (2) and the plate permeability. It should be reiterated that these calculations are based on the assumption of a uniform pseudo-steady region of flow between the reflected shock and the surface of the plate. This is a reasonable assumption that can be inferred from interferometric fringe patterns obtained in the earlier study (Skews and Takayama 1996).

5.2 Flow across the plate

Measurement of the transmitted wave angle is made on that section where the circular waves propagating through the gap have merged into a planar wave and above the point where the corner signal from the model mount influences the flow. Careful measurement shows that a mean line drawn through the front edge of the vortices can intersect the plate ahead of the emergence of the transmitted wave, presumably due to acceleration of gas through the gap. This is shown in Fig. 13. The cylindrical waves ahead of the emerging vortices expectedly slow down before amalgamating with the adjacent waves into a planar wave. This effect results in an initial slight curvature of the line through the vortex street, shown with a white line, which soon settles down, becoming planar, as the transmitted wave also becomes planar. Also shown with white lines is a linear extension of the incident wave. This highlights both the initial

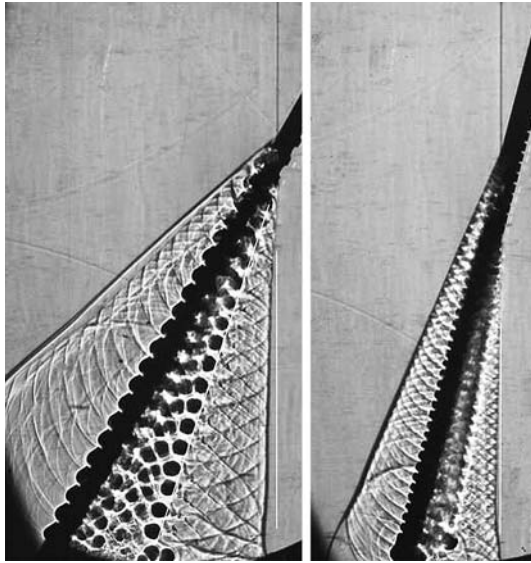


Fig. 13 Flows at wall angles of 60° and 75° with incident Mach numbers of 1.51 and 1.50, and 33% and 67% blockage respectively

merging of the cylindrical waves and the relatively small change in strength of the transmitted wave compared to the incident wave. For the 75° wall, in particular, the transmitted wave is evidently nearly as strong as the incident wave.

The method of analysis for the transmitted wave is similar to that of the flow above the plate, in that the flow is assumed to be pseudo-steady in a frame fixed in the reflection point, and that the flows in the regions are

uniform. Some measure of the validity of this approximation may be gathered from comparing particle path trajectories behind the transmitted wave knowing its angle and Mach number, and the actual path of the vortex street since this represents particle motion. The result is shown in Fig. 14. Although there is significant scatter, the values calculated from the transmitted wave angle are, on average, slightly higher than the measured values. This slight offset thus indicates that the induced flow is slightly slower at the vortex line than the idealisation assumed. The results group according to wall angle as indicated in the figure, with the higher Mach number tests giving higher contact surface angles as is to be expected.

In practical applications where grids such as these are used and may be exposed to shock wave loading, it is clearly of interest to know the load on the screen. Calculation of the pressure difference across the plate, within the pseudo-steady assumptions already made, are therefore pertinent. In this assumption the pressure in region (3) is the same as that in region (4). The pressure difference is non-dimensionalized with respect to the pressure in region (0) and is shown in Fig. 15. For the 100% blockage case the pressure on the back of the plate is assumed to be that in region (0) and the pressure in region (2) is determined from a standard regular reflection calculation. As expected, the pressure difference

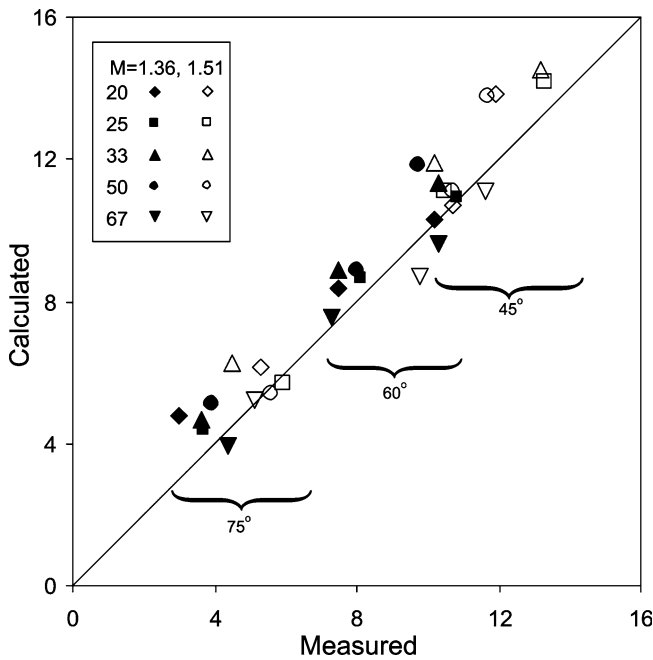


Fig. 14 Variation of contact surface angle calculated from transmitted shock wave and measured from vortex street

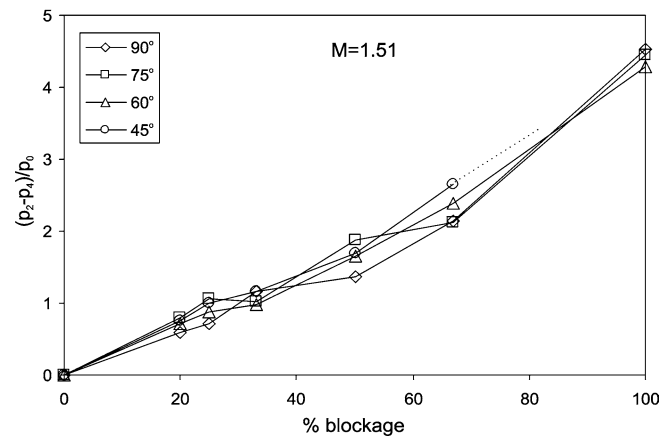
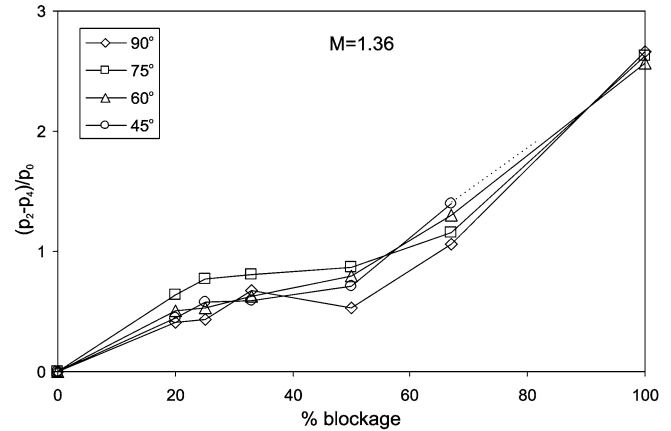


Fig. 15 Variation of the pressure difference across the plate

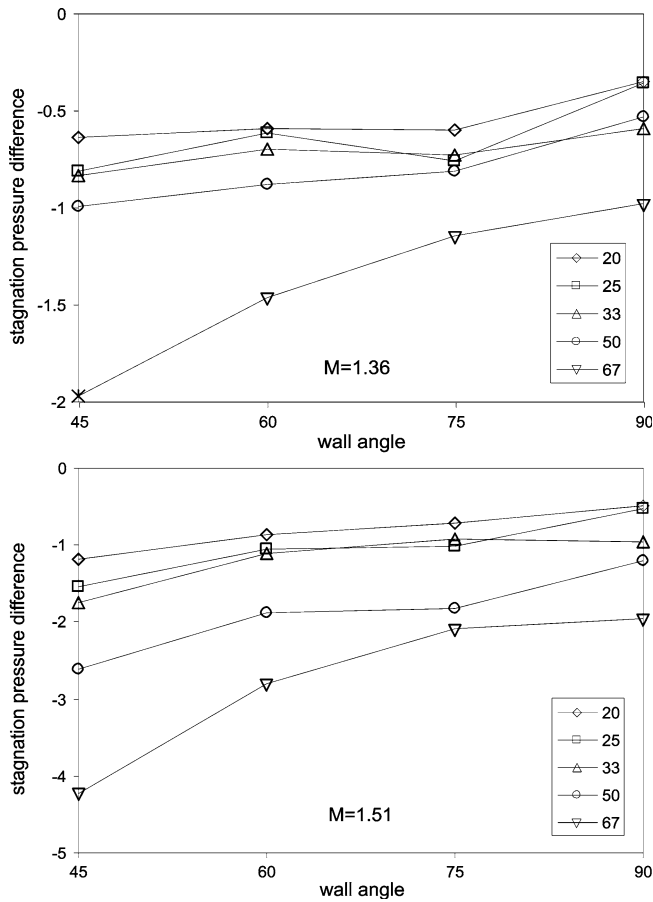


Fig. 16 Stagnation pressure difference as a function of wall angle and blockage percentage

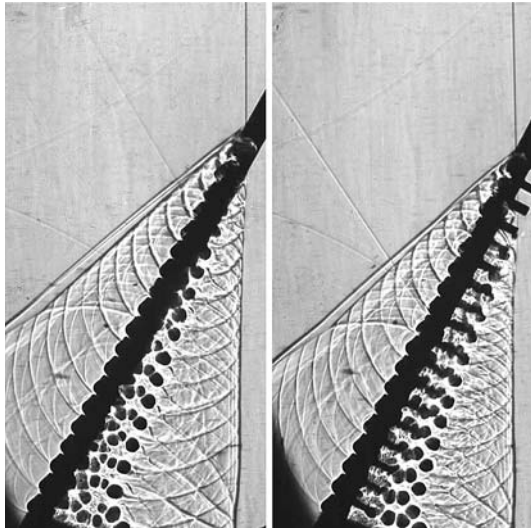


Fig. 17 Similar tests ($M=1.35$, 60° wall, 33% blockage) except for thickness. *Left* 2.4 mm, *Right* 6 mm

increases as the blockage and the Mach number increase. Interestingly, however is that for the 1.36 Mach number there is somewhat of a plateau with blockages

between 20 and 50%. At low blockages the maximum force on the plate occurs for a 75° wall and the minimum for 90° , with the others in between, whereas at 67% blockage it is the 45° case which is highest. These effects are consistent at both Mach numbers and are most probably due to the changing complexities of the flows within the gaps. High resolution simulation would be useful to help to understand these effects, and to see whether they can be replicated. Note that there is no theoretical solution for 100% blockage at a 45° wall angle because it is beyond the extreme angle, i.e. Mach reflection occurs. Experiments with lower blockage give regular reflection, although the point of transition would be difficult to decide because of the complex flow at the gap inlet.

Although it has already been indicated that the transmitted wave has not significantly attenuated with respect to the incident wave (Fig. 13), there are other sources of loss across the plate. One method of quantifying this, within the pseudo-steady frame of reference, is to find the loss of stagnation pressure across the plate. In order to do this the flow properties in state (3) immediately below the plate are needed. An additional assumption is required in order to determine the mean velocity exiting the plate. In Fig. 3 the exiting velocity relative to the plate is V_3^* and is shown as being normal to the plate, i.e. it is assumed that the grids give sufficient guidance to the flow so that it exits parallel to the walls of the gap. Whilst it is apparent that the flow within the gap is complex, both because of the presence of transverse waves and of asymmetric flow separation, some support of this approximation is given by tracking the trajectory of each of the vortices with respect to the gap in which it is originated. This method was also applied in the previous work (Skews and Takayama 1996) and it is found that the vortices do tend to move directly away from the plate, although there is a slight drift parallel to the plate. Detailed studies of vortex trajectories would be useful in order to get a more accurate picture. However, with this assumption the stagnation pressure on either side of the plate may be determined. The corresponding loss, non-dimensionalised with respect to the pressure in region (0) is shown in Fig. 16. As expected the loss is greater for the higher Mach number flows and for the highest blockage, with the loss increasing with decreasing wall angle.

As indicated in Sect. 2 tests were done with plate thicknesses of 2.4, 3.6, 4.8, and 6 mm; all at a blockage of 33% in order to establish whether crossbar aspect ratio would have an effect. The calculated results show no significant differences as regards velocities, pressures, and losses. However, there are visible differences as shown in Fig. 17 for two tests under identical conditions except for the plate thickness. The flows above the plate are very similar but there are distinct differences on the underside, relating both to the wave patterns having apparently more wave components as well as in the configuration of the vortices. These effects are related to the complex interactions within the gaps.

6 Conclusion

A detailed shadowgraph study has been made of the flow induced through grids with various blockage ratios, as the result of shock wave impact. Using a pseudo-steady analysis and the assumption that the flow in each region is uniform, the velocities, pressures and grid losses have been determined. Future work will involve simulation of these flows and will be used to further these studies for more complex geometry, if good correlation with experiment is obtained. Further study of the complex vortex and wave interaction patterns will be undertaken. Both inviscid and viscous codes could be used in order to establish which features are viscous driven.

Acknowledgements The author would like to thank C Law for running some Euler CFD simulations which were used to help

confirm the details of the flow patterns through the grid. Thanks also to H Richter for careful experimentation.

References

- Friend WH (1958) The interaction of a plane shock wave with an inlined perforated plate. UTIA Tech. Note 25. University of Toronto
- Onodera H, Takayama K (1990) Interaction of a plane shock wave with slitted wedges. Expt in Fluids 10:109–115
- Skews BW, Takayama K (1996) Flow through a permeable surface due to shock wave impact. J Fluid Mech 314:27–52
- Onodera H, Takayama K (1990) Shock wave propagation over slitted wedges. Rep Inst Fluid Sci, Tohoku University 1:45–66
- Wilson J, Chima RV, Skews BW (1998) Transmission and incidence losses for a slotted plate. Paper AIAA-98-3252, 34th AIAA/ASME/SAE/ASEE Joint Propulsion Conference, Cleveland, USA. Also available as NASA/TM-1998-207420